Early age autogenous shrinkage cracking risk of an ultra-high performance concrete (UHPC) wall: Modelling and experimental results

J. Kheir, A. Klausen, T.A. A Hammer, L. de Meyst, Benoit Hilloulin, K. van Tittelboom, Ahmed Loukili, N. de Belie

Early Age Autogenous Shrinkage Cracking Risk of an Ultra-High Performance Concrete (UHPC) Wall: Modelling and Experimental Results

J. Kheir[1,2], A. Klausen[3], T.A. Hammer[4], L. De Meyst[1], B. Hilloulin[2], K. Van Tittelboom[1], A. Loukili[2], N. De Belie[1,*]

[1] Magnel-Vandepitte Laboratory for Structural Engineering and Building Materials, Ghent University, Technologiepark Zwijnaarde 60, B-9052 Ghent, Belgium–e-mail: judy.kheir@ugent.be; laurence.demeyst@ugent.be; kim.vantittelboom@ugent.be; nele.debelie@ugent.be
[2] Institut de Recherche en Génie Civil et Mécanique (GeM), Ecole Centrale de Nantes, UMR-CNRS 6183, 1 rue de la Noë, 44321 Nantes, France–e-mail: judy.kheir@ec-nantes.fr; benoit.hilloulin@ec-nantes.fr; ahmed.loukili@ec-nantes.fr
[3] The Norwegian University of Science And Technology-NTNU, N-7491 Trondheim, Norway–e-mail: anja.klausen@ntnu.no
[4] Architecture, Materials and Structures, SINTEF Building and Infrastructure, N-7465 Trondheim, Norway–e-mail: torarne.hammer@sintef.no
* Corresponding author

Abstract

Ultra-High Performance Concrete (UHPC) exhibits high autogenous shrinkage (AS) which significantly increases the risk of early age cracking. To predict the risks of early age shrinkage cracking of environmentally friendly CEM III-based UHPC, a numerical model originally developed for early age crack assessment of ordinary concrete, has been further developed and applied on a demonstration wall with high risk of cracking, cast on a non-deforming slab. The design of the wall was determined through numerical simulation using different parameters, resulting from specific experiments performed on the desired concrete mixture. Early age crack assessment parameters for the model were obtained through different tests performed using the Temperature-Stress Testing Machine (TSTM). Finally, this UHPC wall was built, and occurring strain deformations were recorded in real time using fiber optic (SOFO) sensors embedded in the wall, and measurements taken from demountable mechanical strain gauges (DEMEC). Restrained shrinkage measurements were obtained for the same mixture through ring tests. A comparison between the numerical simulation results and the measurements proved that the proposed model is suitable for UHPC, and the model predicts well the time of crack appearance. Finally, it has been shown that shrinkage values along the wall height are influenced by the degree of restraint.

Keywords: Ultra high performance concrete; modelling; early age crack assessment; autogenous shrinkage; large-scale test

1. Introduction

Predicting the early age cracking risk of cementitious materials is a complicated and difficult task, since there are many properties involved, which develop very fast and highly influenced by temperature (i.e. from heat of hydration) and curing, especially for Ultra High Performance Concrete (UHPC) and High Performance Concrete (HPC). These concrete mixtures are known for their great mechanical and potentially high durability properties that are obtained due to their very low water to cement ratio, generally between 0.2 and 0.3 [1][2]. The high risk of early age cracking is the challenging issue in these durable concretes. Due to the low w/c ratio, UHPCs and HPCs undergo a high Autogenous Shrinkage (AS) driven by a self-desiccation that develops fast during the very early age (within the first days of age). AS, also known as autogenous deformation or basic shrinkage (Eurocode 2), is defined as the external macroscopical volume reduction that occurs under isothermal/sealed conditions, in other words it is the shrinkage that occurs when there is no temperature variation, volume change due to loss or absorbance of substances, or any application of external force [3]. During hardening, the internal relative humidity (RH) will drop and self-desiccation will occur if no external (or internal) water source is present. In mixtures with low water-to-binder ratios, water is rapidly consumed and a dense matrix is formed containing small pores. Hydrostatic tension forces (capillary forces) increase with the increase of smaller pores and lead to the increase in self-desiccation and autogenous shrinkage.. When it comes to UHPCs, RH drops rapidly in a short time to typically reach around 73% at 8 days and 68% after 3 months, while it was found to be 91% at 3 months for ordinary concrete [4]; these values will of course vary from one concrete to another. The previous statement implies that water/vapor filled pores are gradually emptied, and capillary tensions rise on the pore surface which is then perceived as autogenous deformations. As concrete is weak in tension at the early age, it is vulnerable for crack development resulting from high early AS [5][6]. These cracks impair the durability and the functionality of the UHPC structures by letting water with chemical agents and gases infiltrate inducing carbonation, steel corrosion, chemical attack and/or freeze-thaw damage [7]. Thus, in order to limit the cracking risk, it is very important to correctly estimate the evolution of the autogenous shrinkage [8].

Autogenous shrinkage can be measured on cement pastes, mortar and concrete using direct and/or indirect methods. The direct methods measure the volume or the linear autogenous

deformations whereas indirect methods measure in general the relative humidity or the porosity of the cementitious material and correlations will be needed between AS and porosity or RH [9]. The buoyancy method, as developed by Loukili et al. [10], and the capillary tube method [11] are used for volumetric autogenous measurements. Linear autogenous deformations rely on contact and non-contact methods. The corrugated tubes method introduced by Jensen and Hansen [12] is a contact method that combines volumetric and linear deformations with the ability to start the measurement right after casting. Eddy current sensors and laser displacement sensors are considered as non-contact methods for measuring autogenous shrinkage.

Different models were used to evaluate and predict autogenous shrinkage in HPCs. Tazawa and Miyazawa [13] suggested a model that includes the product of the ultimate autogenous shrinkage value, ε_∞(w/cm), and coefficients β(t) and γ, which describe respectively the development rate of AS with time and the effect of cement type. Lee et al. [14] modified the previous model to account for the AS strain that is contributing to the stress development, and applied it on concrete containing mineral additives. Based on the pore structure of the concrete and the capillary tension, Li et al. [15] created a prediction method of early AS of self-consolidating concrete. Model B4 developed by Wan-Wendner et al. [16], is an improved model of the B3 one [17] where prediction was expanded to modern concretes with numerous types of admixtures, and mineral additions as well as the effects of various types of aggregates. Some of these additions increase the shrinkage and creep and others decrease it. The important novelty of the B4 model is the separation of autogenous shrinkage and drying shrinkage.

To predict the early age cracking behavior in massive concrete structures is still a difficult task to perform, because of several complex coupling phenomena such as between the autogenous and thermal strains. In a benchmark study done by Benboudjema et al. [18], different numerical approaches were conducted on multi-scale models (micro- and macroscopic) to predict the early age cracking behavior of a massive concrete structure in external restrained conditions. The study concluded that at the macroscale, a thermo-activation method had to be used in the model in order to have a satisfactory prediction of the adiabatic temperature; while a good prediction of stresses can be achieved if the fast evolution of Young's modulus right after setting time can be estimated. Other physically based numerical model approaches to predict shrinkage of structures have been developed such as *fib* Model Code 2020, a developed version of *fib* MC2010 [19], dealing with both new and existing concrete structures. Another key parameter when it comes to

restrained stress development and corresponding early-age cracking is the time dependent stress response, hereafter denoted creep. Creep can significantly reduce AS- and temperature-induced stresses at early ages: the literature shows a reduction of restrained stresses of as much as 30 – 50% due to the beneficial creep behaviour of concrete [18–21]. However, it should be noticed that temperature-induced compressive creep at very early ages also can contribute to an increase in the succeeding tensile stress development [22-23]. Because of the above described intricate relations between early-age phenomena, an extensive knowledge is needed for the careful calibration and development of models. This is particularly true regarding UHPC whose final properties might considerably depend on their formulation and early age characteristics. Therefore, coupled numerical and experience-based design methods would be particularly beneficial in the scope of tailor-made cementitious materials and structures.

Various approaches at early-age cracking calculations are found in the literature [21], [26]–[33]. Some design approaches are merely an estimation of whether the concrete will crack or not, while other and more complex approaches, chemomechanical [34] thermo-chemo-mechanical [35]or hygro-thermo-chemo-mechanical approaches [36], also provide a prediction of the crack development and the size and rate of occurring crack widths [37]. For all such early-age crack assessments, the accuracy of the outcome is very dependent on the quality and correctness of the models and material parameters used as input [23], [38]–[42]. In the current study, a pragmatic "to crack, or not to crack"-approach was applied [43] by using the special-purpose program CrackTeSt COIN [44]. This approach is considered accurate and advanced, but still practical and easy applicable for contractors and structural designers [45]. In the current study, an early-age crack assessment on a typical restrained wall was performed in CrackTeSt COIN to assess and predict the cracking risk. The model was also used to further determine the conditions necessary to achieve cracking at a specific point of interest in time, around 20 hours after water addition. The combination of a thin wall cast on a stiff base was selected, since this would best provoke cracks by early age shrinkage. The wall was kept thin to minimize the influence of temperature related deformations, and the use of fibres was omitted. The same wall design could then afterwards be used to test the effectiveness of internal curing agents such as superabsorbent polymers to avoid early age cracks. Parameters for the model were obtained through different tests including a test in a Temperature-Stress Testing Machine (TSTM). Then a wall has been built in order to verify the simulated cracking risk through visual observation and deformation

measurements. The real-time occurring strains were recorded automatically with the use of embedded fiber optic sensors and manually with mechanical demountable strain gauges through measuring points glued on the wall. In addition, ring tests were carried out to measure restrained shrinkage, and concrete mechanical properties such as compressive strength and E-modulus were determined.

2. Materials and methods

2.1. Concrete characterization

2.1.1. Introduction

The current sub-section describes the first part of the study: determination of parameters necessary to conduct early age crack assessment of the given concrete. The currently applied methodology for parameter characterization has been verified and thoroughly described in [43]. The results presented in the current section were used to create a material database file representing the given concrete for implementation in CrackTeSt COIN (CTC) [44], where CTC is a two-dimensional special-purpose program for early age crack assessment.

2.1.2. Concrete mix design

The concrete mix design was determined after various optimisation steps, starting from a previously reported mix design [46]. This initial mix design was adapted to the Norwegian situation and made with local Norwegian ingredients (such as aggregates of size 0-8 mm, which are typical in Norway). A blast furnace slag cement CEM III/A 52.5 R (Dyckerhoff Variodur 40) was used in the mix with a dry undensified silica fume (19.8% by weight of cement), and a limestone filler with a quantity of 23.8% by weight of cement. The superplasticizer ViscoCrete UHPC-2 with 40% of active compound was used with a dosage of 1.4% by weight of cement; the water to binder ratio (w/b) equaled 0.2. In the majority of UHPC applications fiber reinforcement is known to be present. In this study, fibers were not used since it was not our goal to increase the flexural or tensile strength. Besides, the mixture design of this study was part of a project [47] where the main focus was rather on the improvement of the matrix itself by internal curing agents known as SAPs (superabsorbent polymers) to achieve crack resistance properties.

Three batches were mixed out of the composition shown in Table 1, batches A, B and C. Batch A was used to determine the hydration heat evolvement of the cement, batch B was used to assess

157 the compressive and tensile strength development, and batch C was used for tests in the Free-
158 Deformation (FD) and the Temperature-Stress Testing Machine (TSTM) systems.

159 Table 1: Concrete mix design

Materials	**(kg/m³)**
Sand 0/4	401.9
Basalt 4-8 mm	649.3
Silica Fume - Elkem Microsilica 940 U	153.8
Cement - Variodur 40 (CEM III/A 52.5 R)	778.2
Filler - Betofill VK50 (limestone)	185.5
Water	186.4
Superplasticizer-SIKA Viscocrete UHPC-2	11.2

160

161 **2.1.3. Testing of Concrete**

162 2.1.3.1. Hydration heat

163 Semi-adiabatic calorimeter tests were performed in a NTNU-box (15 L samples) in order to
164 determine the hydration heat evolvement of the concrete. The NTNU-box comprises a plywood
165 box insulated by 100 mm Styrofoam (with known thermal properties) on all sides. During
166 testing, the box was stored in air at 38 ºC while the air and concrete temperature were measured
167 continuously for 4 days.

168 2.1.3.2. Strength and E-modulus

169 Compressive strength tests were performed on triplicate 100x100x100 mm³ cubes according to
170 NS-EN 12390-3:2009 [48]. Uniaxial tensile strength tests were performed on triplicate
171 100x100x600 mm³ prisms (without notch) in an INSTRON 5985 electromechanical testing
172 system [49], the test set-up is described by Klausen et al. [43]. The main focus in the current
173 study has been early age cracking, and in this perspective, the elasticity modulus in tension is the
174 main parameter. The tensile E-modulus was found from the load-deformation relation measured
175 in the uniaxial tensile strength tests, where the E-modulus was deduced as the stress/strain ratio
176 between 10% and 40% of the failure load.

2.1.4. Model equations and parameters

The maturity principle was applied to describe the effect of curing temperature on the heat and property development of the given concrete. The Arrhenius equation was used as temperature function, and the rate of hydration $H(T_i)$ could consequently be expressed as given in Eq. 1.

$$H(T_i) = exp\left\{\frac{E_T(T_i)}{R} \cdot \left(\frac{1}{293} - \frac{1}{273 + T_i}\right)\right\} \quad Eq.\ 1$$

Where: R (J/(K.mol)) is the gas constant, T_i (°C) is the temperature and E_T (J/mol) is the activation energy: $E_T = A + B(20\text{-}T_i)$, A (J/mol) and B (J/(K.mol)) are model parameters, where B = 0 for T > 20 °C and B has a given value for T < 20 °C

The increase in maturity within a time increment is then $H(T_i) \cdot \Delta t_i$, while the maturity time at a certain concrete age is the sum of all maturity growth increments. For the given concrete, the activation energy parameters A and B were assumed based on experiments with previous concretes having similar properties [50], see Table 2.

The development of compressive strength, tensile strength and E-modulus in tension were modelled by a modified version of the CEB-FIP MC 1990 model, Eq. 2 [51]–[53]. For each property, the model was fitted to the test results by using the method of least squares. The obtained model parameters are presented in Table 2, and illustrated in Figure 3.

$$X(t_e) = X(28) \cdot \left\{exp\left[s \cdot \left(1 - \sqrt{\frac{672 - t_0}{t_e - t_0}}\right)\right]\right\}^n \quad \text{Eq. 2}$$

Where $X(t_e)$ is the property as a function of maturity t_e (MPa if X is equal to f_c or f_t and GPa if it is equal to E), X(28) is the property at 28 days, s and n are unitless curve-fitting parameters (the s-parameter is the same for all properties, while the n-parameter is varying), and t_0 is the starting time for stress development [maturity hours] found from the TSTM-test.

Table 2: Model parameters obtained by using the method of least squares for all tested ages

A	B	t_0	s	n_c	n_t	n_E	f_{c28}	f_{t28}	E_{28}
$[J \cdot mol^{-1}]$	$[J \cdot mol^{-1} \cdot K^{-1}]$	$[h]$					$[MPa]$	$[MPa]$	$[GPa]$

45000	400	8.0	0.141	1.000	0.744	0.323	151.2	6.7	42.8

2.1.5. Testing in the FD and TSTM systems

The currently investigated concrete was tested in the Free-Deformation (FD) system and the Temperature-Stress Testing Machine (TSTM) system. The test set-ups and procedures for these systems are thoroughly described and illustrated in [43], [54], [55].

In the FD system, the autogenous shrinkage of two horizontally oriented and sealed specimens with dimensions of 100x100x500 mm³ was measured. The FD system is temperature-controlled, and the specimens were exposed to 20 °C isothermal conditions during testing. The length measurements were initiated approx. 2 hours after mixing. Autogenous shrinkage was measured up until 289 hours (12 days), and all measurements were zeroed at the starting time for stress development, t_0 = 8 hours (found from the TSTM test).

The TSTM system consists of a dilation rig and a Temperature-Stress Testing Machine (TSTM). The dilation rig measures the free deformation of a horizontally oriented specimen with dimensions of 100x100x500 mm³, while the TSTM is constructed to measure the restrained stress development in the hardening phase for a given degree of restraint. For both rigs, the concrete specimens were carefully sealed with plastic sheets and aluminum foil to prevent any water loss during testing. The TSTM system is temperature-controlled, and the specimens were subjected to a realistic temperature history representing a 50 mm thick concrete wall cast under Norwegian summer conditions, i.e. ambient temperatures of 20 °C.

2.2. Large-scale demonstration wall

2.2.1. Concrete mix design and mixing procedure

Based on the modelling results in section 3.1, the demonstration wall was cast as seen in Figure 1 with the following dimensions: the slab was 2 x 0.95 x 0.2 m³ (l x w x t), and the wall was 1.5 x 2 x 0.05 m³ (h x l x t). To limit the influence of heat produced by the exothermic hydration reaction of cement, the thickness of the wall was kept limited. This was done to minimize the influence of thermal contraction caused by cooling beyond the hydration heat peak, and of thermal gradients which could lead to thermal cracking. The slab was reinforced with two reinforcement meshes (150 mm) of diameter 8 mm positioned with a minimum concrete cover of 25 mm, and the wall with a steel mesh of mesh size 150 mm and diameter 5 mm positioned in

231 the middle of the wall. The slab-wall connection was created using a 1200 mm long steel mesh
232 with a height of 60 mm (mesh size 10 mm and diameter 2 mm) introduced in the slab for 50 mm
233 along the length of the wall and two reinforcement bars (diameter of 12 mm and total length of
234 300 mm), each located at 75 mm from one of the ends. The mesh and the reinforcement bars
235 were placed in the slab by sawing a groove and drilling two holes and subsequently gluing them
236 with epoxy.

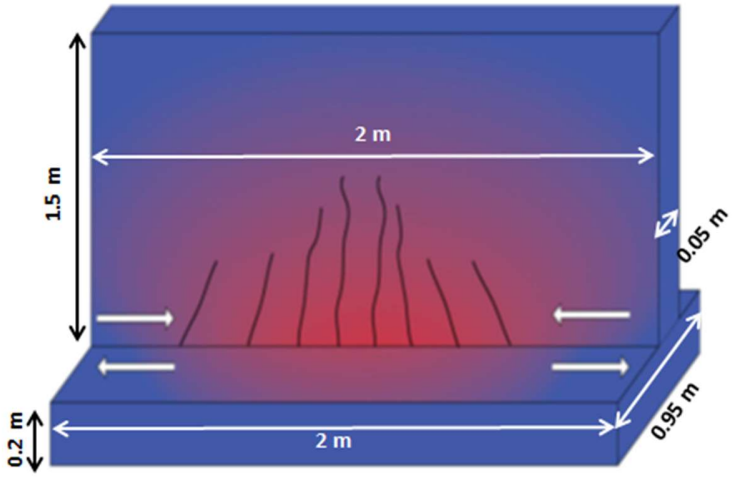

237
238 Figure 1: Schematic representation of the demonstration wall and its dimensions

239 The mix design of the traditional concrete of the slab and mixing procedures of the concrete of
240 both the slab and the wall can be found in

241 Table 3 and Table 4. The mix design of the concrete wall is the same as shown in Table 1. It
242 should be noted that the amount of superplasticizer used (1.1 m% by weight of cement) was less
243 than that used in the batches for the modelling (1.4 m% by weight of cement) to obtain the same
244 slump flow value (700 mm). The slab was cast 3 months prior to the wall and stored at ambient
245 temperature ranging between 7 ºC to 22 ºC, to ensure that the influence of remaining drying
246 shrinkage of the slab could be neglected in the time period considered. The concrete of the slab
247 and the wall were each mixed using a rotating pan mixer Zyklos from the company Pemat-
248 Germany with a capacity of 200 L, a speed of 46 rpm for the rotation of the mixing blades and
249 189 rpm for the pan.

250 Table 3: Mix design composition of the slab

	Slab

Materials	kg/m³
Sand 0/4	670
Gravel 2/8	490
Gravel 8/16	790
Cement-CEM I 52.5N	300
Water	150
Superplasticizer BASF MasterGlenium 51	1.67

Table 4: Mixing procedures for the concrete of both slab and wall

Slab - 5 mins	Wall – 10 mins
Dry mixing for 1 min	Dry mixing for 1 min
Add water while mixing	Add water while mixing
Mixing for 1 min	Mixing for 1 min
Add superplasticizer	Add superplasticizer while mixing and mix for 4 mins
Mixing for 3 mins	Stop at 6 mins and scrape borders for 1 min
	Mixing for 3 mins

The concrete mixture of the wall was poured into the mould from the top with no vibration since it was a self-compacting mixture. Three batches were needed to fill the formwork, with the third batch being mixed 40 minutes after the first one. The pouring of the wall proceeded for 55 minutes and the wall was kept in a climate-controlled room for the whole testing period with a temperature of 20 ± 2˚C and a relative humidity (RH) of 60 ± 5%. At 19 hours after the contact between water and cement, the formwork was removed. No curing was applied after formwork removal. All of the following experiments were additionally performed using these batches except for the ring test which was performed using a separate batch of concrete.

2.2.2. Testing of fresh concrete properties for the wall

2.2.2.1. Slump flow, density and air content

The slump flow was measured according to NBN EN 12350-8 [54]. To determine the density of the fresh self-compacting concrete the method described in NBN EN 12350-6 [56] was followed. The air content of the fresh mixtures was determined using the method described in NBN EN 12350-7 [57].

2.2.2.2. Final setting time

For the final setting time of the mixture, the penetrometer test based on the procedure described in the standard ASTM C 403 [58] was used. This test was used to determine the starting point of the shrinkage measurements.

2.2.3. Hardened concrete properties

2.2.3.1. Compressive strength and E-modulus

The E-modulus and compressive strength tests were determined on triplicate cast cylinders with a height of 300 mm and a diameter of 150 mm according to NBN EN 12390-13 and NBN EN 12390-3, respectively [59], [60]. E-modulus and compressive strength were determined at an age of seven days and 85 days for the wall, and 7 and 28 days for the slab.

2.2.3.2.Shrinkage

Real time deformation behaviour of the wall was measured through fibre optic SOFO sensors (from the company SMARTEC, Switzerland [61]) based on low-coherence interferometry. Sensors were embedded in the wall through attachment to the steel reinforcement mesh before casting. The sensors were mounted at the following three positions: the bottom, the middle and the top annotated respectively as (B), (M) and (T) at a height of 0.120 m, 0.705 m and 1.3 m measured from the slab-wall interface. Five sensors were introduced in the wall, three long sensors with an active length of 1 m (T, M and B2) and two small sensors with an active length of 0.2 m at the bottom edges to monitor AS of the edges: B1 and B3.

After demoulding, on the outer surface of the wall, measurement points for demountable mechanical strain gauges (DEMEC) were glued at three levels following the same pattern as the SOFO positions. At the top, middle and bottom, ten measuring points were glued with a 200 mm spacing between the points, and the first and the last point were 100 mm away from the edges. The DEMEC measurements were taken manually each day for 28 days, and then one

measurement at 60 days and one at 120 days. The positions of the SOFO sensors and the DEMEC points on the wall can be seen in Figure 2.

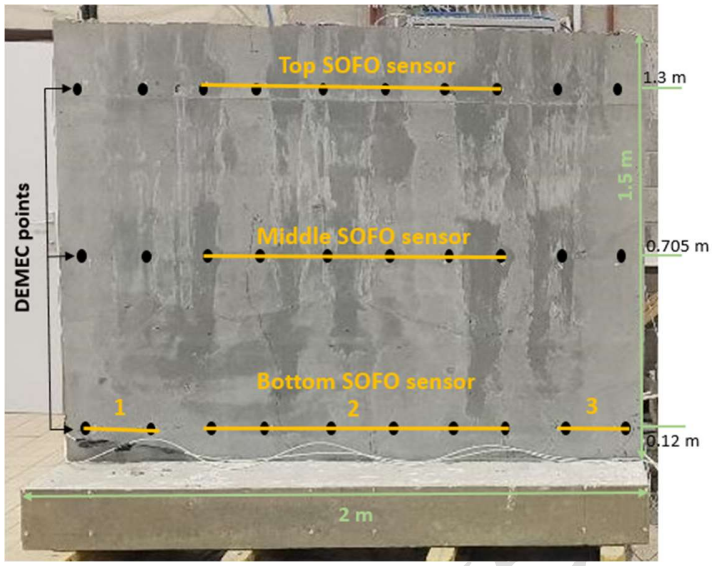

Figure 2: Positions of the embedded fiber optic sensors (SOFO) and the demountable strain gauges points (DEMEC) on the wall

Restrained shrinkage

Restrained shrinkage was investigated according to the method described in the standard ASTM C 1581-04 [62] known as the ring test method. The deformations of the inner steel ring, which represent the strains of the deforming concrete, were measured at three locations through three strain gauges attached to the ring. Measurements were performed every ten minutes from the time of casting until the age of 20 days. The outer steel ring was removed after 19 hours (same time as formwork removal from the wall), and the rings were sealed with plastic foil to avoid water evaporation, and stored in a climate-controlled room at 20 ± 2°C and 60 ± 5% RH.

3. Results

3.1. Concrete characterization

3.1.1. Testing to find the input parameters for the modelling

3.1.1.1. Strength and E-modulus

The obtained compressive strengths, direct uniaxial tensile strengths and the E-moduli in tension are the average of three tested specimens, results are presented in

311 Table 5. The tensile E-modulus was found from the load-deformation relation measured in the
312 uniaxial tensile strength tests, where the E-modulus was deduced as the stress/strain ratio
313 between 10% and 40% of the failure load.

314 Table 5: Strength and E-modulus of the concrete

Compressive strength*		**Tensile strength****		**E-modulus in tension****	
Time [h]	f_c **[MPa]**	**Time [h]**	f_t **[MPa]**	**Time [h]**	E_c **[GPa]**
24	68.9	27	3.9	27	34.8
120	126.7	72	5.7	72	39.1
670	149.3	696	6.6	696	42. 6

315 ** cube strength, 100x100x100 mm³ cubes*
316 *** prism strength, 100x100x600 mm³ prisms*

317 3.1.1.2. Hydration heat

318 The box was stored in air at 38 ºC while the air and concrete temperature were measured
319 continuously for 4 days. The hydration heat evolvement results are presented in Figure 3.

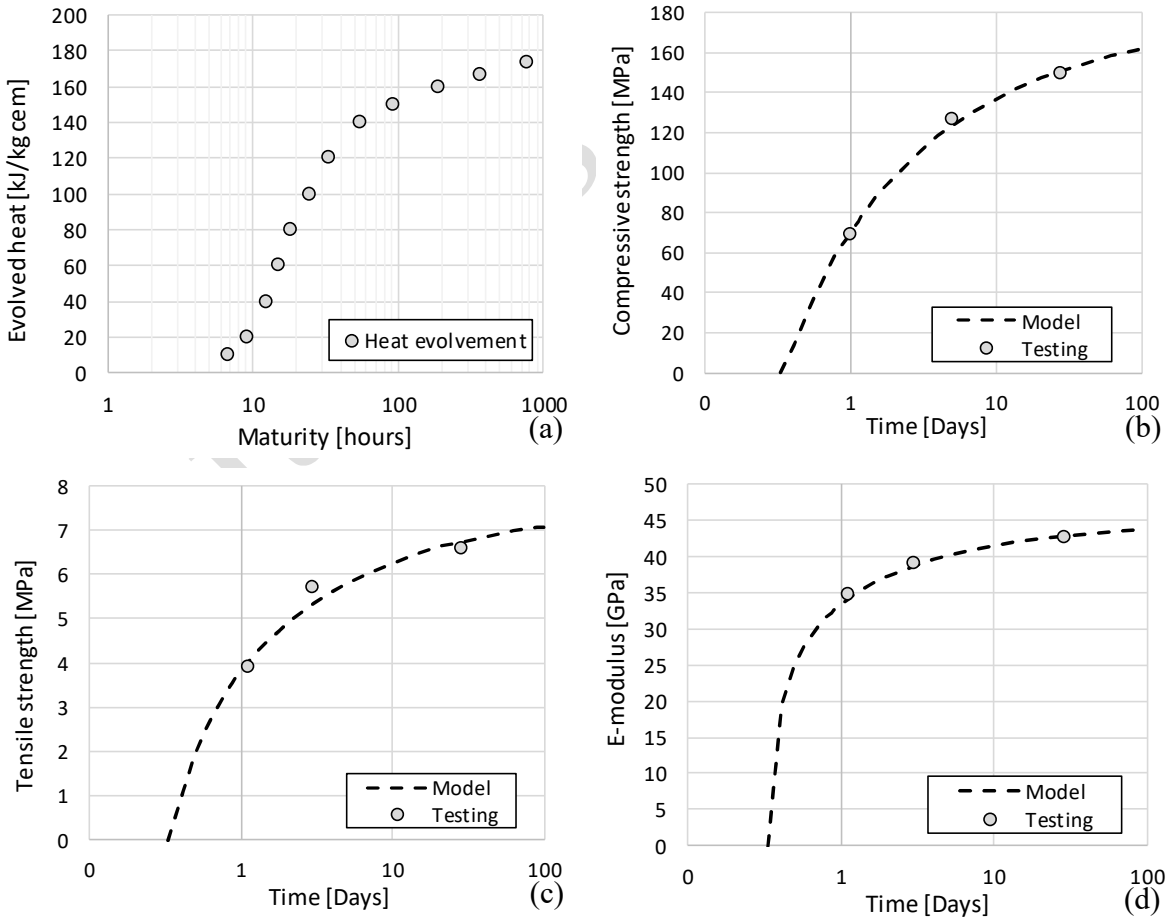

Figure 3: Hydration heat evolvement (a). Laboratory test results versus model: compressive strength (b), tensile strength (c) and E-modulus (d)

3.1.2. Autogenous shrinkage measured in Free Deformation (FD) and Temperature Stress Testing Machine (TSTM)

Autogenous shrinkage was measured up until 289 hours (12 days), and all measurements were zeroed at the starting time for stress development, t_0 = 8 hours (found from the TSTM test). Autogenous shrinkage measured in the FD system, i.e. under 20 °C isothermal curing conditions, is provided in Figure 4 (a). The result represents the average measurements of two concrete specimens.

The TSTM system is temperature-controlled, the applied temperature history, Figure 4 (b), was determined using the program CTC, and it was based on the calorimetric heat evolvement test results and the geometry of a pre-defined wall.

The TSTM test was performed in order to determine material- and model parameters for early age crack assessment in CTC. A degree of restraint of only 30% was chosen in order to minimize the restrained stresses during testing, and hence to keep the test running as long as possible to obtain enough data for parameter estimation. The measured stress development of the concrete when subjected to realistic temperature conditions and a degree of restraint of 30% is presented in Figure 4 (b). The specimen developed failure in tension at 4.1 MPa after only 26 hours (51 hours of maturity), which is a somewhat lower tensile strength level than found from the corresponding uniaxial tensile strength tests. It should however be noticed that the specimen in the TSTM test was subjected to both realistic temperature conditions and sustained loading prior to failure, i.e. there were considerable variations in the test conditions between the tensile strength test and the TSTM test.

In addition to autogenous shrinkage and stress development, tests in the TSTM system also provided the starting time for stress development, t_0, the incremental E-modulus development and the coefficient of thermal expansion, CTE, for the concrete in question. The starting time for stress development t_0 was found from the restrained stress development test as the maturity time when the measured stress reached 0.1 MPa for tests performed under realistic temperature conditions. After testing, the CTE was determined by applying temperature steps of ±3 °C around an initial temperature of 20 °C. The CTE was determined as the average value over four

such temperature loops. The CTE for the current concrete was found to be 10.7 x 10^{-6}/°C after 250 hours of maturity (10 days of maturity).

The autogenous shrinkage for the concrete subjected to a realistic temperature history was deduced by subtracting the thermal dilation (calculated by the CTE and the measured temperature) from the total free deformation measured in the dilation rig. The autogenous shrinkage is given in Figure 4 (a), where the curve was zeroed at the starting time for stress development, t_0 = 8 hours. The autogenous shrinkage development was observed to be quite similar for both 20 °C isothermal and realistic temperature curing conditions, Figure 4 (a).

In the current study, the time-dependent behavior of the concrete has been described by viscoelasticity for ageing materials, and more specific, by the double power law [63]. The creep model parameters ϕ_0, d and p were deduced by the following procedure: The restrained stress development measured in the TSTM was back-calculated by a calculation routine in Excel. The performed stress calculations were based on linear viscoelasticity with age adjusted effects, using the degree of restraint, the measured temperature and free deformation from the dilation rig as input data. The creep parameters were estimated based on previous experience on similar concretes, and then adjusted by fitting the calculated stress development to the measured stress development, Figure 4 (b). The creep model parameters deduced for the current concrete were: ϕ_0 = 0.70, d = 0.42 and p = 0.26. The stress development is driven by thermal dilation (TD) and autogenous deformation (AD). Usually, the temperature increase causes an initial compression and appurtenant compressive stress. In the current case, the AD is so high it outcompetes the temperature effect and causes a tensile stress from the start. Between 10 and 12 hours, the AD rate is somewhat lower, and the sum of AD and TD is close to zero. Hence the stress development between 10 and 12 hours is very small due to the lack of volume changes in this period.

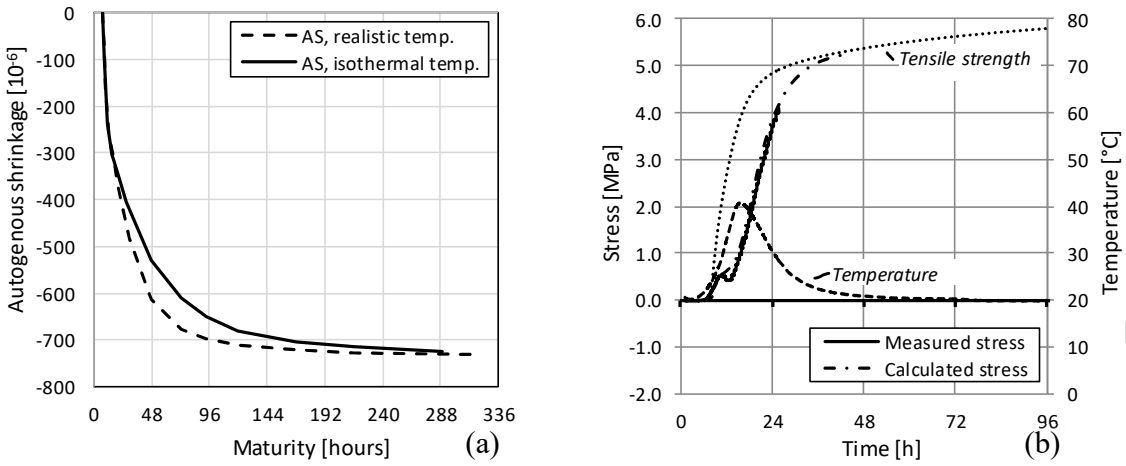

Figure 4: Autogenous shrinkage measured in the FD (isothermal) and the TSTM-system (realistic temperature evolution), zeroed at t_0 (a); Stress development in the TSTM, realistic curing temperature, R = 30% (b)

3.2. Modelling

A model was established in the program CrackTeSt COIN (CTC) [44] in order to simulate the temperature-, stress- and strength development in the planned UHPC demonstration wall described in the previous section,

Figure 5 (a). The main aim was to assess and predict the cracking risk in the wall, and to determine further the conditions necessary to achieve cracking at around 20 hours after water addition. CTC is a two-dimensional special-purpose program for temperature- and stress calculations in young hardening concrete. A crack risk simulation in CTC comprises a heat flow analysis followed by a structural analysis. Stress computations in the structural analysis include stresses in the orthogonal direction according to the boundary conditions given by the user. The heat and the structural analysis use the same element mesh generated by CTC

Figure 5 (b). All in all, CTC provides a crack assessment of a given structure by simulating the temperature- and stress development, as well as the time and location where the generated stress exeeds the corresponding tensile strength.

The wall geometry was modelled as defined in the previous section, see

Figure 5 (a). The ambient temperature and the fresh concrete temperature were assumed to be 23 °C and 20 °C, respectively. The restraint conditions, which vary over the wall height, were defined by CTC based on the geometry of the structure and the applied concrete. The investigated concrete was implemented in CTC by a material database file created from the laboratory test program presented in the previous section. It should be noticed that the program

uses autogenous deformation measured in the laboratory versus maturity as input, and does not include the effect of drying. The reason for this is that CTC is generally used for massive structures, where the effect of drying can be neglected. The variation parameters in the currently performed analyses were "type of formwork" as well as "formwork removal time", which both affect the temperature development, and hence the cracking risk, in the wall. Analyses were run for the wall subjected to three different formwork alternatives:

- 20 mm plywood removed at 18 hours
- 20 mm plywood removed at 72 hours
- 50 mm plywood removed at 72 hours

The CTC calculation results are presented in Figure 6, where each graph represents an average value over the hatched area of the wall as illustrated in
Figure 5 (a). The hatched area is 50x50 mm² and it is located 150 mm up in the wall when measured from the top of the slab. The restraint is highest close to the underlying foundation, while the temperature increase is highest further up in the wall. The highest stress development is found at the most unfortunate combination of high restraint and high temperature, which for massive walls is considered to be approximately one wall thickness up from the top of the slab [53], [64]. For the current wall, CTC found this location to be at the hatched area illustrated in
Figure 5 (a).

Simulated temperature developments for the three formwork alternatives are presented in Figure 6 (a). The thicker formwork, 50 mm plywood, provided better insulation and hence a higher temperature increase and decrease during curing. For the alternatives with 20 mm plywood, an earlier "formwork removal time" resulted in a somewhat steeper temperature decrease during the cooling period.

The simulated stress developments (average over the hatched area) were quite similar over the first 22 hours for all three formwork alternatives, Figure 6 (b). For the given concrete, the early age volume changes are strongly dominated by a very high autogenous deformation (AD). Consequently, a small variation in the curing temperature will only constitute a limited influence on the total early age volume changes, and hence the stress development. The difference in peak temperature between the cases of 50 and 20 mm plywood formwork, is approximately 6 to 7 °C. With a CTE of around 10.7 x 10^{-6}/°C, this causes a difference in thermal strain of about 60-70 microstrain between the different formworks. The AD at the same time is -420 microstrain. This

makes clear that for UHPC, AD is the main driving force for stress development, and a difference of 60-70 microstrains caused by temperature does not have a big influence on the stress development. The increase in tensile strength was slightly higher for the 50 mm plywood alternative due to its higher temperature increase during curing, however, the correspondingly higher temperature-decrease during the cooling phase also caused a somewhat higher stress development over time when compared to the other alternatives, Figure 6 (b). For the wall cast with 20 mm plywood formwork removed at 18 hours after water addition, the generated tensile stress in the hatched area exceeded the corresponding tensile strength at approximately 18 hours after water addition. The cracks will initiate in the wall center, and they have to achieve a certain width to be seen with the naked eye. However, at 20 hours after water addition, it is expected that cracking can be observed for the given demonstration wall.

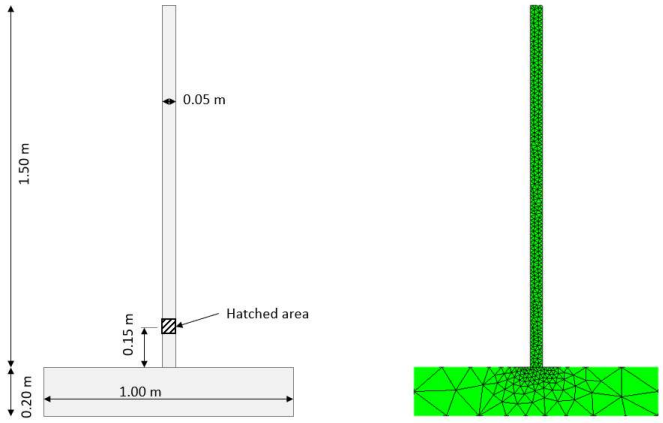

(a) (b)

Figure 5: Demonstration wall model for use in CTC (a) and generated mesh (b)

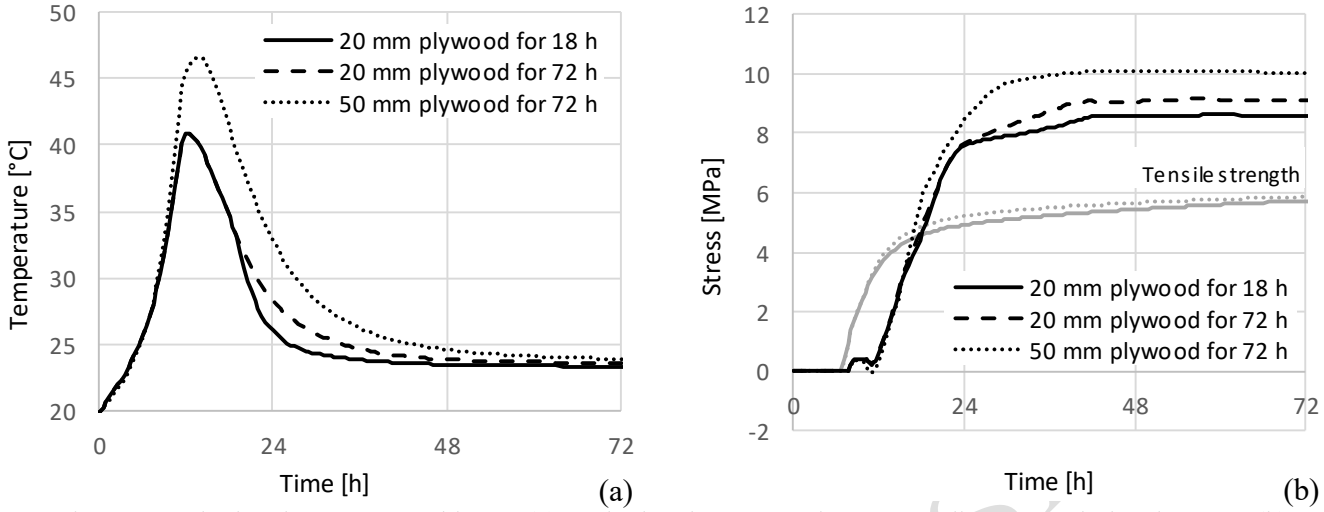

Figure 6: Calculated temperature history (a); Calculated stress- and corresponding strength development (b)

3.3. Large-scale demonstrator

3.3.1. Fresh concrete properties

The slump flow of the wall was equal to 706 ± 22 mm, with an air content of 2.7% and a final setting time of 5.5 hours. The values represented are the average of the results obtained from the three batches used for the wall except for the final setting time which was performed only on one batch.

3.3.2. Hardened concrete properties

3.3.2.1. Compressive strength and E-modulus

The mechanical properties of the concrete used for the demonstration structure (slab + wall) can be found in Table 6. Note that the measured compressive strength of 87.2 MPa at 7 days of age is significantly lower than that of the concrete tested for the numerical simulation input (section 2.1.3.2) being 126.7 MPa at 5 d of age. This large difference is confirmed by testing at later ages too: at 85 d of age the cylinder strength for the demonstration wall was 121 MPa, while the cube strength of the concrete used for the model input was 149 MPa at 28 days of age. Different specimen geometry (150/300 mm cylinders vs 100 mm³ cubes), is probably one reason for a lower value, as it is known that cubes give generally higher measured strength values, in the order of 5 to 10 percent in UHPC [65]. In addition, several comprehensive studies on high strength concrete [55], [66], [67] concluded that strength values of 100 mm³ cubes were on average 11-12 % higher than those of 150/300 mm cylinders. Furthermore, in an old Belgian

standard [68], a general formula has been used to estimate with an accuracy of 10% the ratio between the compressive strength obtained from a 150/300 mm cylinder, R_x , to the compressive strength obtained from a cube of 100 mm³, R_{w10}. The ratio corresponding to the cylinders used in this study is $\frac{R_x}{R_{w10}} = 0.75$. Therefore, if we consider the strength value of 121 MPa obtained for the wall on cylinders, it would correspond to a value of 161 MPa on 100 mm³ cubic specimens, showing that the differences between cube and cylinder strength can indeed be large.

Table 6: Mechanical properties of the concrete used for the demonstration wall (on cylinders, d=150 mm and h=300 mm)

	Compressive strength (MPa) 7 days	**E-modulus (GPa) 7 days**	**Compressive strength (MPa) 28 or 85 days**	**E-modulus (GPa) 28 or 85 days**
Slab	48.8 ± 0.7	-	57.6 ± 2.2 (28 d)	39 ± 8 (28 d)
Wall	87.2 ± 5.7	48	121.1 ± 3.5 (85 d)	47 (85 d)

3.3.2.2. Shrinkage

Measurements of the real-time occurring strains in the wall were obtained automatically from the fibre optic SOFO sensors embedded inside the wall and are represented in Figure 7. The measurements were recorded during 4 months to follow the whole period of active shrinkage (as it can be seen on the shrinkage curves there is no big difference in terms of deformations between the third and the fourth month), the curves represent the values recorded from the long sensors with an active length of 1 m. But since the early age cracking risk is discussed in this study, it is interesting to consider especially the first few days of the concrete age. Thus, shrinkage values over the first 8 days obtained from the long and one short fiber optic sensor are represented in Figure 7 on the right. Measurements from the second short sensor (B3 in Figure 2) could not be presented as there was too much noise in the obtained results. As it can be seen from the shrinkage curves, the top of the wall shrinks more than the middle and more than the bottom, demonstrating the influence of the restraining condition at the bottom, i.e. the wall cannot freely shrink at this location. At around one day, deformation curves transform from a

very high rate of shrinkage deformations to a much lower shrinkage rate. With water being rapidly consumed at early age, deformations are expected to increase in low water-to-binder ratio concrete. After few hours, rigidity of UHPC becomes quickly high which restrains the following deformations. At the age of 8 days shrinkage values of -130 µm/m, -320 µm/m, -640 µm/m and -815 µm/m were obtained for bottom 1, bottom 2, middle and top, respectively. At 120 days, shrinkage values obtained from the long sensors were -540 µm/m, -910 µm/m and -1110 µm/m for the bottom, the middle and the top, respectively.

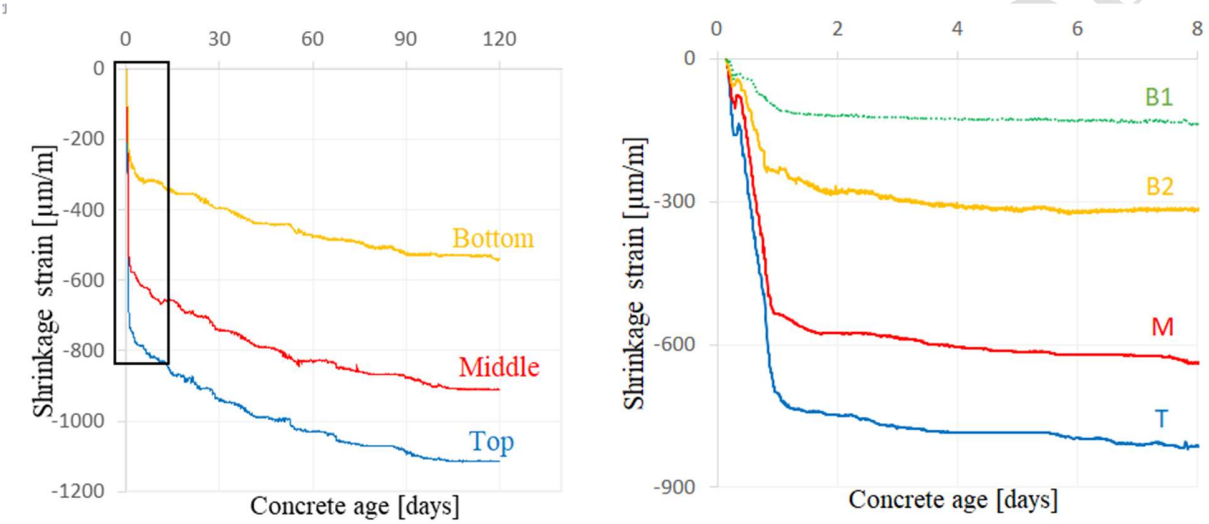

Figure 7: Deformations of the top (T), the middle (M) and the bottom (B2) of the wall obtained from the long fiber optic sensors embedded inside starting from t0 equal to the final setting time = 5.5 hours for a period of 4 months (on the left); on the right a zoomed graph over the first 8 days of the deformations in addition to the deformation curve given by the short sensor B1

Shrinkage strain curves obtained from the demountable strain gauges measurements were also in accordance with the results found from the fiber optic sensors as it can be seen in Figure 8. The starting point of the DEMEC measurements is taken equal to 23h30 after water-cement contact, since the points needed to be glued on the wall after formwork removal (the zero point on the time axis is the contact moment between water and cement). Over the 4 months period of testing, it was confirmed that the wall has shrunk more at the top than the bottom; a value of 360 µm/m is reached for the top, 330 µm/m for the middle and 250 µm/m for the bottom. In Figure 9 the results from the SOFO measurements are compared with the ones obtained from the DEMEC measurements over the first 28 days, during which regular DEMEC measurements were taken. The curves were plotted from an age of 23h30 after water-cement contact (the time where the

first DEMEC measurements were obtained), and the two sensor types followed the same behavior over 28 days.

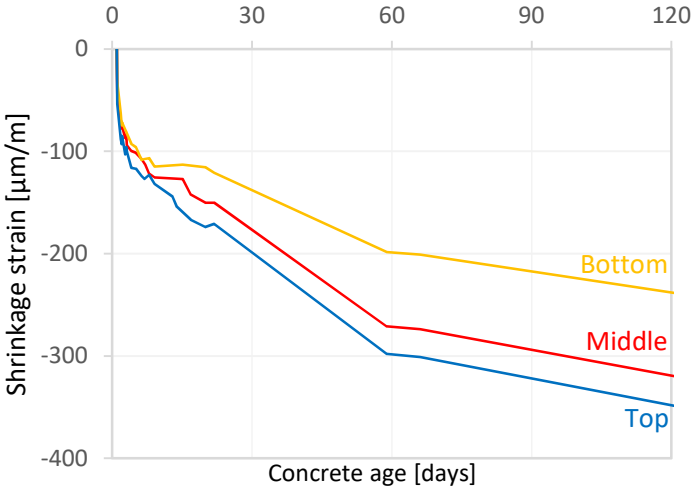

Figure 8: Deformation measurements obtained from the demountable strain gauges (DEMEC) starting at an age of 23.5h after water-cement contact

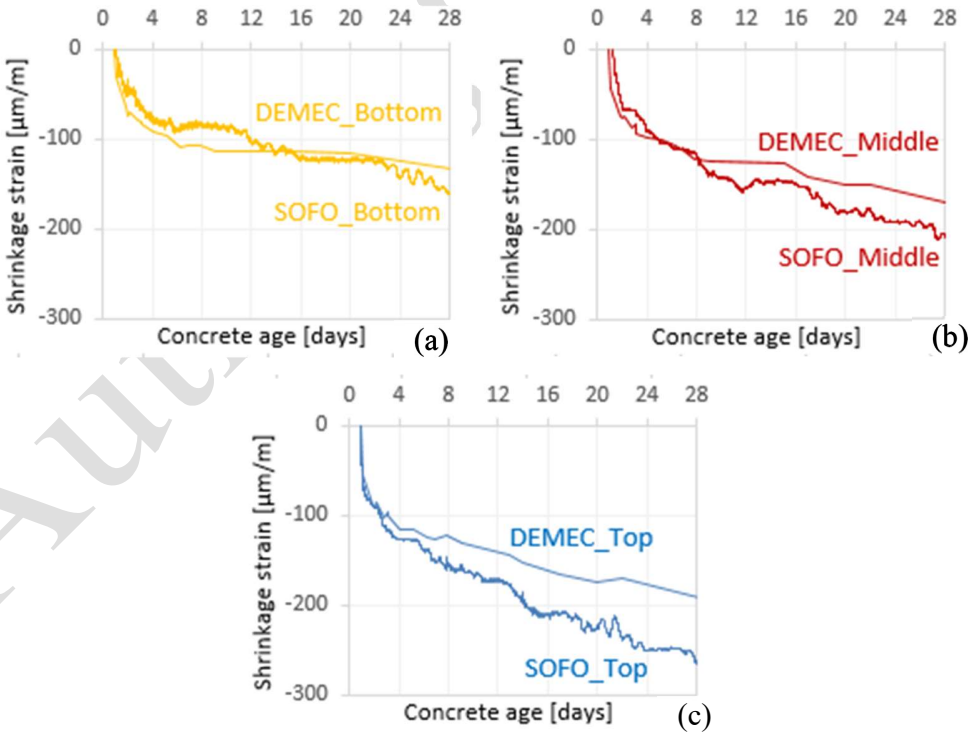

Figure 9: Comparison of the occuring shrinkage strain results obtained from the fiber optic SOFO sensors and the demountable strain gauges (DEMEC), starting at an age of 23.5h after water-cement contact (a) is for the bottom, (b) for the middle and (c) for the top positions on the wall

Restrained shrinkage

The results of the restrained shrinkage test are presented in Figure 10, each curve represents the values obtained from the sensors attached to the ring (one sensor was not working properly therefore only two out of three are shown). Time zero is equalled to the water-cement contact and the curves are plotted from the age of one hour. The sudden jump in the curve represents the time of cracking, where the sensors measure an abrupt change. The strain values reached about -100 µm/m before the sample cracked at around 2 days.

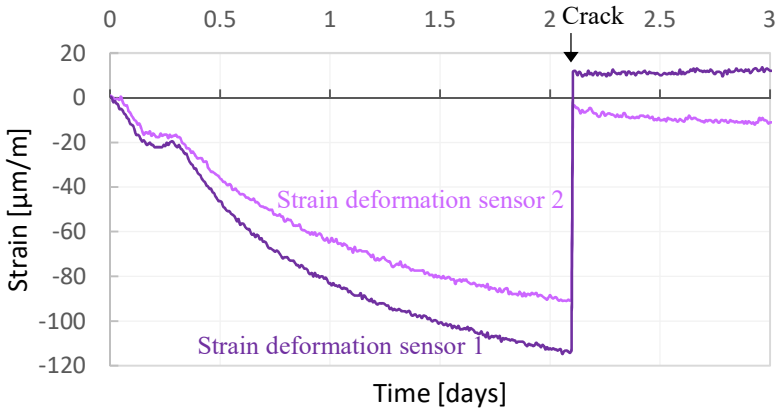

Figure 10: Restrained shrinkage results obtained from the ring method; the zero point on the time axis represents the moment of water-cement contact

4. Discussion

4.1. Comparison of stress development and time of cracking

The work comprises three different approaches to determine stress development and subsequent cracking assessment:

a) TSTM test with 30% restraint
b) Numerical simulation of the wall
c) Strain measurements and visual observation of the wall

The TSTM test measured the stress development in the hardening phase for a specimen subjected to a degree of restraint of 30%. This restraint did not represent the given demonstration wall, but it was applied in order to minimize the restrained stress during testing, i.e. to keep the test running as long as possible to obtain enough data for parameter estimation. Despite the low restraint, the TSTM specimen developed failure in tension as early as 26 hours after water addition, confirming that the investigated concrete is very prone to early age cracking.

541 The degree of restraint in a wall varies over the wall height and length, and it depends on several
542 parameters: the area, the geometry and the stiffness of both the wall and the base slab, the elastic
543 properties of the ground beneath, the length to height ratio of the wall, as well as possible slip
544 failures between the wall and the base slab. The wall deformation measurements in Figure 7 and
545 illustrate how the restraint in the wall decreases with increasing distance from the joint, i.e.
546 increasing deformations with increasing distance from the base slab; this represents the very
547 typical relation between restraint and the distance from the base as reported by Schleeh [69],
548 **Erreur ! Source du renvoi introuvable.**where several tests were conducted on micro-concrete
549 walls with different length-to-height ratios cast on a steel slab. For a wall cast on a massive
550 concrete base it is suggested by BS 8110 2 [70] that the restraint factor at the joint lies between
551 0.6 and 0.8. This corresponds well with a simplified calculation method presented by CIRIA
552 C766 [33], which estimated the given wall to have a degree of restraint at the joint of 0.78, i.e.
553 78%. The same calculation estimated a degree of restraint of 30% to occur approx. 550 mm
554 above the joint. In the TSTM test, the specimen reached a tensile stress of 4.1 MPa after 26
555 hours, Figure 5. Correspondingly, the CTC simulations showed a restrained stress of approx. 4.8
556 MPa after 26 hours in an area 550 mm above the joint. Although these approaches were not fully
557 comparable due to variations in their temperature histories as well as the restraint considerations
558 discussed in the following section, they did provide restrained stresses in the same order of
559 magnitude, indicating rather good agreement.
560 The first crack in the demonstration wall was reported two hours after formwork removal (21
561 hours after water-cement contact). This was a through-going crack that reached the middle height
562 of the wall, followed by other non through-going cracks (except at the edges) as depicted in
563 Figure 11. The CTC stress simulation estimated the generated tensile stress in the critical part of
564 the wall to exceed the corresponding tensile strength somewhat earlier, at approx. 18 hours after
565 water addition. However, the given demonstration wall has a low length to height ratio $L/H = 1.3 < 3$, meaning that the Bernoulli-Euler assumption of “plane sections remain plane when
567 deforming” cannot be applied. This may cause 3D effects in terms of a reduction of restraint and
568 hence stresses in the wall, and these effects may not be captured by the two-dimensional CTC
569 simulation. Consequently, due to the low length to height ratio of the wall, the CTC simulation
570 was expected to provide a somewhat higher restraint and stress development than the actual wall.
571 In addition, the demonstration wall seemed to experience some slip failure between the wall and

the base slab, Figure 11, which also reduces the degree of restraint. Summarized, the degree of restraint in the demonstration wall was expected to be somewhat lower than the degree of restraint determined by CTC in the simulations, i.e. the stress development and cracking of the wall was expected to occur somewhat later than estimated by the simulation. The program CTC, which is intended for massive concrete structures, does not include the effect of drying. Drying shrinkage is generally not considered to have a big influence on UHPC/HPC structures, and in addition, the analysis expects the first crack to appear at approx. 18 hours after water addition, which is the same time as formwork removal. Before 18 hours, the formwork will prevent drying, and hence the possible drying-induced inaccuracy of the simulation prior to the first crack can be neglected. All things considered, the simulated stress development and crack assessment showed good agreement with the observations of the demonstration wall.

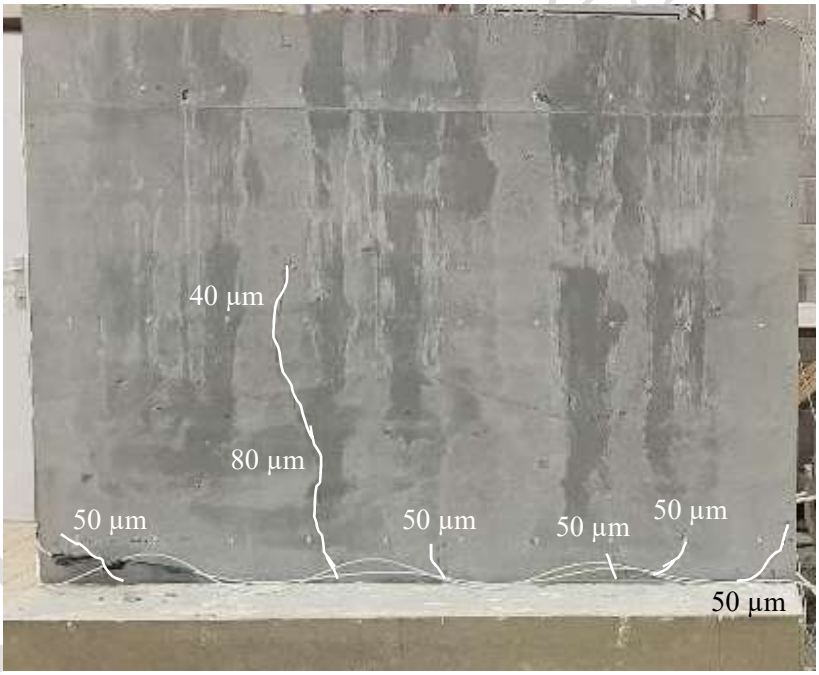

Figure 11: Crack development on the wall with the approximated crack width at each position

In addition, regarding the ring test, the observed jumps in Figure 10 represent cracking of the rings that took place at around 2 days after water-cement contact, a cracking time that was later than that for the wall. The main reason is the huge difference in the experimental set-up between the ring and the wall, e.g. the geometries and restraining conditions, that highly influence the

induced stresses. In addition, the wall also experienced larger additional thermal contraction following the hydration heat peak.

4.2. Shrinkage measurements

The work comprises four different deformation measurements:

a) Free deformation measured in the FD-system (isothermal)
b) Free deformation measured in the TSTM-system (realistic temperature)
c) Shrinkage strains occurring in the wall under various restraint conditions, measured with two different systems (realistic temperature)
d) Restrained shrinkage deformations measured in the ring test (isothermal)

AS was measured under 20 °C isothermal conditions in the FD-system, and under realistic temperature conditions in the TSTM-system. Both measurements were zeroed at the starting time for stress development, t_0 = 8 hours, as determined from the TSTM test. The AS development was observed to be quite similar for both 20 °C isothermal and realistic temperature curing conditions, Figure 4 (a), as opposed to other concretes where realistic curing temperature regimes have been found to initiate fundamental differences in the AS development when compared to 20 °C isothermal curing [71]. The free deformation measurements in the TSTM-system include both autogenous deformation and thermal dilation. The demonstration wall was rather thin, with a thickness of only 50 mm, however, due to the high cement content and corresponding heat evolvement, the given wall experienced a temperature increase of as much as 20 °C during curing. This caused a thermal expansion and contraction of about 200 microstrains, which still was far less than the deduced AS which reached a level of 700 microstrains after approximately one week. It is thus evident that the considerable amount of AS found for the investigated concrete constitutes the main mechanism when it comes to early age volume changes and hence the cracking risk of the demonstration wall.

Under surrounding temperature (20 ± 2°C and 60 ± 5% RH), real-time deformations of the wall were measured automatically by the fiber optic SOFO sensors and manually by the demountable DEMEC strain gauges. In Figure 7, results obtained from the SOFOs are plotted where the influence of the restraining condition at the bottom is clearly shown. The wall undergoes a lot of shrinkage strains at the top where it is more free to shrink with less stresses. Then, these strains gradually decrease when approaching the restraining condition at the bottom near the slab-wall

connection. On the left of Figure 7, a big difference is seen between the shrinkage values of the bottom sensor and the middle/top sensors, as the shrinkage strain difference between the top and the middle is around 200 µm/m whereas the one between the middle and the bottom is around 400 µm/m. The behavior of the bottom curve was studied at the very early age (0-24h) as seen in Figure 12, and a change of the slope of the shrinkage strain curve was seen at around 19 hours which equals to 21 hours after water-cement contact (taking into account a gap of 2 hours that represents the time to cast the wall and to put the sensors into operation). The abrupt change in Figure 12 represents the formation of the cracks, which was seen with the naked eye 2 hours after formwork removal (formwork was removed at 19 hours after water-cement contact). The longest and first crack passed through the bottom sensor, for that reason there was a relaxation of the stresses at that location which explains the big difference between the bottom and the middle-top strain curves. At the final measurement (120 days after casting of the wall) this crack had a length of 850 mm and a width of 180 µm at the bottom of the wall. Halfway the crack height the width was 80 µm and at the top of the crack the width was 40 µm. Using the same interpretation, the shrinkage values of the bottom sensor B1 near the edge of the wall were 23% lower than for the long bottom sensor 2 in the middle, due to the presence of many cracks that were clearly apparent at the edges of the wall. Since B1 had more cracks over its smaller length, it measured less strain deformations than B2.

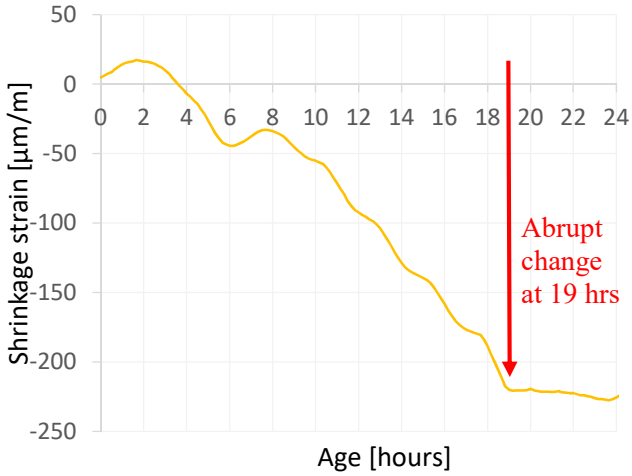

Figure 12: Representation of the shrinkage measurements obtained from the long bottom fiber optic sensor embedded inside of the wall at the early age (24 h)

Shrinkage strains of the wall were also manually measured with demountable strain gauges. Values are shown in Figure 8 over a period of 4 months (same as for the SOFOs). These curves

644 follow the same trend as the SOFOs and also show the influence of the restraining condition at
645 the bottom. The ranges of the DEMEC values at the end of the testing period are lower than the
646 ranges of strains of the SOFOs (Figure 7), which is due to the difference in the starting point of
647 the measurements. For the DEMEC measurements, points need to be glued on the wall after
648 formwork removal and first measurements are taken after the glue dried which was roughly
649 around 3.5 hours after formwork removal. Therefore, measurements started after 23.5 hours
650 when a big part of the occurring strains had already happened. A comparison between the SOFO
651 and DEMEC measurements for the first 28 days of age was performed in Figure 9. The starting
652 point of the measurements in this figure was taken to be 23.5 hours after water-cement contact
653 for both techniques. The SOFO measurements showed slightly higher strain values at the
654 different levels. Drying shrinkage is normally not considered to have a big influence on
655 UHPC/HPC structures. Zhang et al. found that most of the total shrinkage undergone by high
656 strength concrete (containing silica fume) could be attributed to AS rather than drying shrinkage
657 due to the dense and impermeable matrix [72]. Xie et al. performed autogenous and free total
658 shrinkage on UHPC prisms and showed that drying shrinkage comprises approximately 20% of
659 the total measured shrinkage. In addition, during early concrete ages (until 7 days after water to
660 cement contact), drying shrinkage is not considered since the difference between the free total
661 and autogenous shrinkage curves is negligible [73]. Nevertheless, water evaporation near the
662 surface of the wall could have been faster than deeper inside the matrix, which could have led to
663 a slightly lower level of cement hydration and therefore slightly lower shrinkage strains obtained
664 from DEMEC measurements. In addition, the rapid water evaporation at the surface will enhance
665 the formation of microcracks which leads to a relaxation of stresses around the crack itself. This
666 also justifies the lower DEMEC shrinkage strain curves.
667 The ring test method was used to evaluate the shrinkage under restrained conditions. As it can be
668 seen in Figure 10, samples reached a strain of -120 μm/m before cracking after 2 days. Under
669 realistic temperature and RH conditions (20 ± 2°C and 60 ± 5% RH), the wall cracked two hours
670 after formwork removal at around 21 hours after water-cement contact while rings cracked at a
671 later age. This could be justified by the fact that the wall experienced larger additional thermal
672 contraction following the hydration heat peak in addition to the differences in geometry and
673 restraining conditions existing between the wall and the ring.

5. Conclusion

To predict the risks of early age shrinkage cracking for UHPC, a numerical model, which has been established primarily for normal concrete, has been further developed and applied on a demonstration wall with high risk of cracking, cast on a non-deforming slab. Thus, an early age crack assessment was performed in this study using a numerical simulation model applied on a typical restrained wall. A demonstration structure (a wall cast on a non-deforming slab) has then been built in order to verify the simulated cracking risk through visual observation of cracking and deformation measurements of the wall. A comparison between the numerical simulation results and the actual measurements was presented. The currently used UHPC showed a considerable autogenous shrinkage, constituting the main driving mechanism to the early age volume changes and the corresponding high cracking risk of the investigated wall.

The following conclusions can be drawn:

- The comparison between the numerical simulation results and the actual measurements proved that the proposed model is suitable for UHPC-concrete. A good fit between the model and experimental results was found for the development of compressive strength, tensile strength and E-modulus in tension. In addition, the performed tests and analyses confirmed that UHPCs are very prone to early age cracking due to the high AS development as well as the high temperatures generated during curing even though the wall was rather thin. Indeed, the model highlighted the increased risk of cracking due to the increased degree of restraint associated with the small wall thickness.
- The numerical simulation gave a good prediction of the cracking risk in the wall: cracking was predicted to appear at approximately 20 hours after water addition, and the first crack was observed in the wall at 21 hours after contact between cement and water. Hence, the novelty of the model remains in the time prediction of crack development rather than the crack development itself. The through-going crack observed in the demonstration wall reached the mid height of the wall with a width of 180 µm at its bottom, 80 µm at its middle and 40 µm at its top. The crack was followed by other similar small cracks with a width of 50 µm.
- Autogenous shrinkage results under isothermal and realistic conditions followed the same behavior and experimental and modelled results were in the same range. Under realistic

conditions the occurring strains in the wall were recorded automatically using fiber optic sensors embedded inside the wall and manually with demountable strain gauges through points glued on the outer surface of the wall. Another key point to stress on, AS deformations can be measured in different ways for big/massive structures where it was shown that AS is very dependent on the zeroing time of measurements as well.

- Restrained shrinkage tests were performed on the cast concrete using the ring test method. Rings cracked at 2 days, a later time than the wall, which is probably because the wall experienced larger additional thermal contraction following the hydration heat peak in addition to the effect of a difference in geometry and restraining conditions that exists between the ring and the wall.

Acknowledgement

These results are part of a project that has received funding from the European Union's Horizon 2020 research and innovation programme under grant agreement Nº685445 – LORCENIS and from the Research Foundation Flanders (FWO Vlaanderen) under project No G.0A28.16. The authors gratefully acknowledge the support and provision of materials from Dirk Qvaeschning and Sara Irico (Dyckerhoff GmbH). The data that support the findings of this study are available from the corresponding author upon reasonable request.

6. References

[1] D. P. Bentz, O. M. Jensen, K. K. Hansen, J. F. Olesen, H. Stang, and C. J. Haecker, "Influence of Cement Particle-Size Distribution on Early Age Autogenous Strains and Stresses in Cement-Based Materials," *J. Am. Ceram. Soc.*, vol. 84, no. 1, pp. 129–135, 2001, doi: 10.1111/j.1151-2916.2001.tb00619.x.

[2] V. Baroghel-bouny *et al.*, "Autogenous Deformations of Cement Pastes : Part II . W/C effects , Micro-Macro Correlations , and Threshold values," 2006.

[3] L. Wu, N. Farzadnia, C. Shi, Z. Zhang, and H. Wang, "Autogenous shrinkage of high performance concrete: A review," *Construction and Building Materials*, vol. 149. 2017, doi: 10.1016/j.conbuildmat.2017.05.064.

[4] A. Loukili, A. Khelidj, and P. Richard, "Hydration kinetics, change of relative humidity, and autogenous shrinkage of ultra-high-strength concrete," *Cem. Concr. Res.*, vol. 29, no. 4, pp. 577–584, 1999, doi: 10.1016/S0008-8846(99)00022-8.

[5] V. Mechtcherine and H.-W. Reinhardt, *Application of Superabsorbent Polymers (SAP) in Concrete Construction*. 2012.

[6] L. De Meyst, J. Kheir, J. R. Tenório Filho, K. Van Tittelboom, and N. De Belie, "The use of superabsorbent polymers in high performance concrete to mitigate autogenous

shrinkage in a large-scale demonstrator," *Sustain.*, vol. 12, no. 11, 2020, doi: 10.3390/su12114741.
[7] P. Lura, K. Van Breugel, and I. Maruyama, "Effect of curing temperature and type of cement on early-age shrinkage of high-performance concrete," *Cem. Concr. Res.*, vol. 31, pp. 1867–1872, 2001.
[8] A. Darquennes, S. Staquet, and B. Espion, "Determination of time-zero and its effect on autogenous deformation evolution," *Eur. J. Environ. Civ. Eng.*, vol. 15, no. 7, pp. 1017–1029, 2011, doi: 10.1080/19648189.2011.9695290.
[9] Z. Hu *et al.*, "A review on testing methods for autogenous shrinkage measurement of cement-based materials," *J. Sustain. Cem. Mater.*, vol. 2, no. 2, pp. 161–171, 2013, doi: 10.1080/21650373.2013.797937.
[10] A. Loukili *et al.*, "A New Approach to Determine Autogenous Shrinkage of Mortar at Early Age Considering Temperature History," *Cem. Concr. Res.*, pp. 0–8, 2017.
[11] E.-I. Tazawa and S. Miyazawa, "Influence of cement and admixture on autogenous shrinkage of cement paste," *Cem. Concr. Res.*, vol. 25, no. 2, pp. 281–287, 1995.
[12] O. Mejlhede Jensen and P. Freiesleben Hansen, "A dilatometer for measuring autogenous deformation in hardening portland cement paste," *Mater. Struct.*, vol. 28, no. 7, pp. 406–409, 1995, doi: 10.1007/BF02473076.
[13] E. Tazawa and S. Miyazawa, "Effect of constituents and curing condition on autogenous shrinkage of concrete," in *Autogenous Shrinkage of Concrete*, London: E & FN Spon, 1999, pp. 267–280.
[14] H. K. Lee, K. M. Lee, and B. G. Kim, "Autogenous shrinkage of high-performance concrete containing fly ash," *Mag. Concr. Res.*, vol. 55, no. 6, pp. 507–515, 2003, doi: 10.1680/macr.2003.55.6.507.
[15] Y. Li and J. Li, "Capillary tension theory for prediction of early autogenous shrinkage of self-consolidating concrete," *Constr. Build. Mater.*, vol. 53, pp. 511–516, 2014, doi: 10.1016/j.conbuildmat.2013.12.010.
[16] R. Wendner, M. H. Hubler, and Z. P. Bažant, "The B4 model for multi-decade creep and shrinkage prediction," *Mech. Phys. Creep, Shrinkage, Durab. Conrete A Tribut. to Zdenek P. Bazant - Proc. 9th Int. Conf. Creep, Shrinkage, Durab. Mech. CONCREEP 2013*, no. September 2013, pp. 429–436, 2013, doi: 10.1061/9780784413111.051.
[17] Z. P. Bažant and S. Baweja, "Justification and refinements of model B3 for concrete creep and shrinkage 1. statistics and sensitivity," *Mater. Struct.*, vol. 28, no. 7, pp. 415–430, 1995, doi: 10.1007/BF02473078.
[18] F. Benboudjema *et al.*, "COST TU1404 benchmark on macroscopic modelling of concrete and concrete structures at early age: Proof-of-concept stage," *Constr. Build. Mater.*, vol. 174, pp. 173–189, 2018.
[19] J. Walraven and A. Bigaj-van Vliet, *fib Model Code for Concrete Structures 2010*, no. October. 2013.
[20] D. Bosnjak, "Self-induced Cracking Problems in Hardening Concrete Structures," Norwegian University of Science and Technology, 2000.
[21] S. Altoubat A and D. Lange, "Creep, Shrinkage, and Cracking of Restrained Concrete at Early Age," *Mater. J.*, vol. 98, no. 4, pp. 323–331, 2001.
[22] D. S. Atrushi, "Tensile and Compressive Creep of Early Age Concrete : Testing and Modelling," Norwegian University of Science and Technology, 2003.
[23] G. De Schutter, "Applicability of degree of hydration concept and maturity method for

thermo-visco-elastic behaviour of early age concrete," *Cem. Concr. Compos.*, vol. 26, no. 5, pp. 437–443, 2004, doi: 10.1016/S0958-9465(03)00067-2.
[24] F. Benboudjema and J. M. Torrenti, "Early-age behaviour of concrete nuclear containments," *Nucl. Eng. Des.*, vol. 238, no. 10, pp. 2495–2506, 2008, doi: 10.1016/j.nucengdes.2008.04.009.
[25] D. Schlicke and N. V. Tue, "Consideration of Viscoelasticity in Time Step FEM-Based Restraint Analyses of Hardening Concrete," *J. Mod. Phys.*, vol. 04, no. 10, pp. 9–14, 2013, doi: 10.4236/jmp.2013.410a2002.
[26] R. Springenschmid, "Prevention of Thermal Cracking in Concrete at Early Ages - Preface," London, Great Britain, 1998. doi: ISBN 9780367447670.
[27] G. De Schutter, "Fundamental study of early age concrete behaviour as a basis for durable concrete structures," *Mater. Struct.*, vol. 35, no. 245, pp. 15–21, 2002.
[28] F. Czerny, K. Van Breugel, and E. A. B. Koenders, "The reliability of crack predictions for hardening concrete structures," in *Proceedings of the International Conference on Cement Combinations for Durable Concrete*, 2005, pp. 757–766, doi: 10.1680/ccfdc.34013.0083.
[29] J. Guomin, "Cracking Risk of Concrete Structures in The Hardening Phase," Norwegian University of Science and Technology (NTNU), 2008.
[30] I. Pane and W. Hansen, "Predictions and verifications of early-age stress development in hydrating blended cement concrete," *Cem. Concr. Res.*, vol. 38, no. 11, pp. 1315–1324, 2008, doi: 10.1016/j.cemconres.2008.05.001.
[31] F. Barre *et al.*, *Control of Cracking in Reinforced Concrete Structures: Research project CEOS.fr*. France, 2016.
[32] A. B. E. Klausen, "Early age crack assessment Codes , guidelines and calculation methods D. WP1.2 (Ed.) DaCS Project Report No 2," Trondheim, Norway, 2018.
[33] P. Bamforth, *Control of cracking caused by restrained deformation in concrete (C766)*. CIRIA, 2018.
[34] R. Lackner and H. A. Mang, "Chemoplastic material model for the simulation of early-age cracking: From the constitutive law to numerical analyses of massive concrete structures," *Cem. Concr. Compos.*, vol. 26, no. 5, pp. 551–562, 2004, doi: 10.1016/S0958-9465(03)00071-4.
[35] M. Cervera, J. Oliver, and T. Prato, "Thermo-Chemo-Mechanical Model For Concrete. II: Damage and Creep," *J. Eng. Mech.*, no. September, pp. 1028–1039, 1999, doi: http10.1061/(ASCE)0733-9399(1999)125:9(1028).
[36] D. Gawin, F. Pesavento, and B. A. Schrefler, "Hygro-thermo-chemo-mechanical modelling of concrete at early ages and beyond. Part II: Shrinkage and creep of concrete," *Int. J. Numer. Methods Eng.*, vol. 67, no. 3, pp. 332–363, 2006, doi: 10.1002/nme.1636.
[37] G. P. A. G. van Zijl, R. de Borst, and J. G. Rots, "A numerical model for the time-dependent cracking of cementitious materials," *Int. J. Numer. Methods Eng.*, vol. 52, no. 7, pp. 637–654, 2001, doi: 10.1002/nme.211.
[38] P. Morabito, "Methods to Determine the Heat of Hydration of Concrete," in *Prevention of Thermal Cracking in Concrete at Early Ages*, R. Springenschmid, Ed. Munich, Germany: CRC Press, 1998.
[39] O. M. Jensen and P. F. Hansen, "Influence of temperature on autogenous deformation and relative humidity change in hardening cement paste," *Cem. Concr. Res.*, vol. 29, no. 4, pp. 567–575, 1999, doi: 10.1016/S0008-8846(99)00021-6.

[40] Z. P. Bažant, "Prediction of concrete creep and shrinkage: Past, present and future," *Nucl. Eng. Des.*, vol. 203, no. 1, pp. 27–38, 2001, doi: 10.1016/S0029-5493(00)00299-5.
[41] T. Kanstad, T. A. Hammer, Ø. Bjøntegaard, and E. J. Sellevold, "Mechanical properties of early age concrete: Evaluation of test methods for tensile strength and modulus of elasticity. Determination of model parameters. IPACS report," Sweden, 2001.
[42] M. Nilsson, "Restraint Factors and Partial Coefficients for Crack Risk Analyses of Early Age Concrete Structures," Luleå University of Technology, Sweden, 2003.
[43] A. E. Klausen, T. Kanstad, and Ø. Bjøntegaard, "Hardening Concrete Exposed to Realistic Curing Temperature Regimes and Restraint Conditions : Advanced Testing and Design Methodology," *Adv. Mater. Sci. Eng.*, vol. 2019, p. 15, 2019, doi: 10.1155/2019/9071034.
[44] "JEJMS Concrete AB, CrackTeSt COIN (2009-2012)." Luleå, Sweden.
[45] "COIN: Concrete Innovation Centre - a centre for research based innovation.," *Research Council of Norway*, 2007. https://www.sintef.no/en/projects/coin/coinp (accessed Sep. 23, 2019).
[46] "Sustainable Building with Ultra-High Performance Concrete. Main report from the German Priority Program 1182 of the German Research Foundation: Heft 22 Structural Materials and Engineering Series, UNI Kassel, Germany Ed.: M. Schmidt et al., 2014.," Kassel, Germany, 2014.
[47] L. De Meyst, J. Kheir, J. R. Tenório Filho, K. Van Tittelboom, and N. De Belie, "The use of superabsorbent polymers in high performance concrete to mitigate autogenous shrinkage in a large-scale demonstrator," *Sustain.*, vol. 12, no. 11, 2020, doi: 10.3390/su12114741.
[48] "NS-EN 12390-3, Testing hardened concrete - Part 3: Compressive strength of test specimens, Standard Norge, Norway," 2009.
[49] Instron, "INSTRON 5980 Series, Norwood, MA, USA," 2019. .
[50] Ø. Bjøntegaard, "Thermal Dilation and Autogenous Deformation as Driving Forces to Self-Induced Stresses in High Performance Concrete," Norwegian University of Science and Technology (NTNU), Trondheim, Norway, 1999.
[51] "CEB-FIP Model Code 1990: Design code, Comité Euro-International du Béton, 0727716964, 9780727716965, Lausanne, Switzerland," 1991.
[52] T. Kanstad, T. A. Hammer, Ø. Bjøntegaard, and E. J. Sellevold, "Mechanical properties of young concrete: Part II: Determination of model parameters and test program proposals," *Mater. Struct.*, vol. 36, no. 4, pp. 226–230, 2003, doi: 10.1007/bf02479615.
[53] Ø. Bjøntegaard, "Basis for and practical approaches to stress calculations and crack risk estimation in hardening concrete structures – State of the art," 2011.
[54] Bureau voor Normalisatie, "NBN EN 12350-8: Testing fresh concrete - Part 8: Self-compacting concrete - Slump-flow test," in *NBN - EN*, 2019.
[55] M. Imam, L. Vandewalle, and F. Mortelmans, "Are current concrete strength tests suitable for high strength concrete?," *Mater. Struct.*, vol. 28, no. 7, pp. 384–391, 1995, doi: 10.1007/BF02473073.
[56] Bureau voor Normalisatie, "NBN EN 12350-6 : Testing fresh concrete - Part 6: Density," in *NBN - EN*, 2019.
[57] Bureau voor Normalisatie, "NBN EN 12350-7 : Testing fresh concrete - Part 7: Air content - Pressure methods," in *NBN - EN*, 2019.
[58] American Society of Testing and Materials, "Standard Test Method for Time of Setting of Concrete Mixtures by Penetration Resistance," in *Annual Book of ASTM Standards*, vol.

878 04, 1999, pp. 1–6.
879 [59] Bureau voor Normalisatie, “NBN EN 12390-13: Beproeving van verhard beton - Deel 13:
880 Bepaling van de secans- elasticiteitsmodulus bij druk,” in *NBN - EN*, no. september, 2005,
881 p. 149.
882 [60] Bureau voor Normalisatie, “NBN EN 12390-3 : 2019 Testing hardened concrete - Part 3 :
883 Compressive strength of test specimens,” in *NBN - EN*, 2019.
884 [61] SMARTEC, “Standard SOFO Deformation Sensor.” .
885 [62] American Society of Testing and Materials, “Standard Test Method for Determining Age
886 at Cracking and Induced Tensile Stress Characteristics of Mortar and Concrete under
887 Restrained Shrinkage,” in *Annual Book of ASTM Standards*, West Conshohocken, PA,
888 2004.
889 [63] Z. P. Bažant and E. Osman, “Double power law for basic creep of concrete,” *Mater.
890 Struct.*, vol. 9, no. 1976, pp. 3–11, 1976, doi: 10.1007/BF02478522.
891 [64] T. Kanstad, D. Bosnjak, and J. A. Øverli, “3D Restraint Analyses of Typical Structures
892 with Early Age Cracking Problems, IPACS report,” Sweden, 2001.
893 [65] B. A. Graybeal, “Material Property Characterization of Ultra-High Performance
894 Concrete,” *Fed. Highw. Adm.*, no. FHWA-HRT-06-103, p. 186, 2006.
895 [66] S. Smeplass, “High Strength Concrete, SP4. Material Design. Report 4.4-Mechanical
896 Properties- Normal Density Concrete,” Trondheim, Norway, 1989.
897 [67] M. Held, “Research results concerning the properties of high-strength concrete,”
898 *Darmstadt Concr. Annu. J.*, vol. 5, pp. 71–78, 1990.
899 [68] “NBN B 15-220; 1970 (NF)-Influence des Dimensions et Formes de l’éprouvette sur la
900 Résistance à la Compression du Béton,” .
901 [69] W. Schleeh, “Die Zwangspannungen in einseitig festgehaltenen Wandscheiben,” *Beton-
902 und Stahlbetonbau*, vol. 57, no. 3, pp. 64–72, 1962.
903 [70] C. Civil Engineering and Building Structures Standards Committee, “Part 2: Code of
904 practice for special circumstances.,” in *BS 8110-2: Structural use of concrete*, London,
905 UK, 1985.
906 [71] A. E. Klausen, T. Kanstad, Ø. Bjøntegaard, and E. J. Sellevold, “The effect of curing
907 temperature on autogenous deformation of fly ash concretes,” *Cem. Concr. Compos.*, vol.
908 109, no. January 2019, 2020, doi: 10.1016/j.cemconcomp.2020.103574.
909 [72] M. H. Zhang, C. T. Tam, and M. P. Leow, “Effect of water-to-cementitious materials ratio
910 and silica fume on the autogenous shrinkage of concrete,” *Cem. Concr. Res.*, vol. 33, no.
911 10, pp. 1687–1694, 2003, doi: 10.1016/S0008-8846(03)00149-2.
912 [73] T. Xie, C. Fang, M. S. Mohamad Ali, and P. Visintin, “Characterizations of autogenous
913 and drying shrinkage of ultra-high performance concrete (UHPC): An experimental
914 study,” *Cem. Concr. Compos.*, vol. 91, no. August, pp. 156–173, 2018, doi:
915 10.1016/j.cemconcomp.2018.05.009.
916